Available online at www.sciencedirect.com
ScienceDirect
Trans. Nonferrous Met. Soc. China 35(2025) 1233−1248
Transactions of Nonferrous Metals Society of China
www.tnmsc.cn

Mechanism of property enhancement of Cu−Ti alloys via microalloying with Cr and Mg elements

Huan WEI[1], Hong-li WEI[2], Hua-yun DU[2], Qian WANG[2], Cai-zhi ZHOU[3], Ying-hui WEI[2], Li-feng HOU[2]

1. College of Aeronautics and Astronautics, Taiyuan University of Technology, Taiyuan 030024, China;
2. College of Materials Science and Engineering, Taiyuan University of Technology, Taiyuan 030024, China;
3. College of Engineering and Computing, University of South Carolina, Columbia, SC 29208, USA

Received 1 February 2024; accepted 4 September 2024

Abstract: The effect of adding Cr and Mg on the microstructure and properties of Cu−Ti alloys was examined. Cu−Ti−Cr−Mg alloys were fabricated using vacuum induction melting. The microstructure and phase composition of Cu−Ti−Cr−Mg alloys in different aging states were characterized. Additionally, the hardness and electrical conductivity of the materials were investigated. Results show that the precipitation pattern in Cu−Ti−Cr−Mg alloys resembled that of binary Cu−Ti alloys, with Cr and Ti forming the intermetallic compound of Cr_2Ti during casting. The introduction of Cr and Mg increased the hardness of the alloy. Increasing the Mg content in the Cu−Ti−Cr−Mg alloy led to grain refinement and fast nucleation of continuous precipitates during the early aging stage. Moreover, the addition of Mg impeded discontinuous precipitate growth by segregating along the precipitate surfaces. Consequently, the Cu−4Ti−0.5Cr−1Mg alloy exhibited limited discontinuous precipitates at the grain boundaries and a gradual decline in hardness during the over-aging period.

Key words: Cu−Ti alloy; microalloying element; discontinuous precipitates; precipitation hardening

1 Introduction

The miniaturization of electronic components requires enhanced performance, particularly strength, of copper alloys [1]. Cu−Be alloys are widely used in electronics because they offer high strength and excellent electrical conductivity [2]. Nevertheless, health hazards in the production of Cu−Be alloys have considerably stimulated the abandonment of their usage [3]. Consequently, Cu−Ti alloys, noted for their exceptional mechanical properties, are considered ideal substitutes for Cu−Be alloys [4,5]. However, Cu−Ti alloys typically exhibit lower electrical conductivities than Cu−Be alloys [6].

Researchers have explored the addition of a third microalloying element to enhance the overall performance of Cu−Ti alloys. Various elements such as Al [7] and Co [8] enhance the electrical conductivity of Cu−Ti alloys while compromising their strength. However, with the introduction of Ni, a NiTi intermetallic compound is formed with Ti, which improves the electrical conductivity and reduces the hardness [9]. When the Ni content is increased to 3 wt.%, Ti reacts with Ni to generate precipitation phases of Ni_3Ti, leading to the improvements in both the hardness and electrical conductivity of the alloy [10]. MARKANDEYAS et al [11] and HUANG et al [12] have demonstrated that the addition of Cr element leads to an increase in the hardness, tensile strength, and conductivity of the Cu−Ti alloy. LIU et al [13] explores the

Corresponding author: Ying-hui WEI, Tel: +86-351-6018685, E-mail: yhwei_tyut@126.com;
Li-feng HOU, Tel: +86-351-6018683, E-mail: houlifeng78@126.com
DOI: https://doi.org/10.1016/S1003-6326(24)66745-2

microstructure and performance of Cu−3Ti−2Mg alloy. The addition of Mg enhanced both the strength and conductivity of the alloy. Additionally, the investigation conducted by SAITO et al [14] revealed that the majority of the Mg solute exhibits uniform distribution within the matrix region, with a minor fraction being present in the precipitate phase. Furthermore, the inclusion of Mg leads to an improvement in the tensile performance of the material when compared to the binary Cu−Ti alloy.

According to the aforementioned research findings, the addition of a third microalloying element provides only modest improvements in Cu−Ti alloy performance. Current research is now directed towards multi-element microalloying strategies. For instance, LIU et al [15] studied the aging-hardening behavior of a cold-rolled Cu−3Ti−3Ni−0.5Si alloy, noting the development of Ni_2Si, Ni_3Si, and Ni_3Ti precipitates. LI et al [16] reported that a combination of pre-aging, cold rolling, and final aging on Cu−2.7Ti−0.15Mg−0.1Ce−0.1Zr achieved a strength of 1035 MPa and conductivity of 20.1% (IACS). WANG et al [17] applied multi-stage thermomechanical treatments to Cu−2.57Ti−0.35Cr−0.11Mg−0.04Si alloy, enhancing strength to 1144 MPa and conductivity to 24.1% (IACS). Furthermore, HUANG et al [18] demonstrated that the addition of Fe significantly improves the high-temperature performance, plasticity, and oxidation resistance of Cu−8Ti−0.4Cr−0.4Mg alloys. Moreover, the equal channel angular pressing of Cu−2.5Ti−0.4Cr−0.1Mg resulted in a substantial strength enhancement [19].

Researchers have primarily focused on investigating the modifications in Cu−Ti alloy performance resulting from multi-element micro-alloying. However, exploration of multi-element interaction mechanisms remains relatively scarce. Cr and Mg are known to have an advantageous influence on the comprehensive properties of Cu−Ti alloys. In the present investigation, we deliberately selected Cr and Mg and adopted composition ratios extensively explored by previous scholars. Cu−4Ti−0.5Cr−0.5Mg, Cu−4Ti−1Cr−0.5Mg, and Cu−4Ti−0.5Cr−1Mg alloys were meticulously designed and fabricated to systematically explore their micro-structure, phase transformation sequence, mechanical properties, and physical properties. The objective is to comprehensively elucidate the interaction mechanisms between Cr and Mg in Cu−Ti alloys.

2 Experimental

The materials used in this study were melted in a vacuum induction furnace with the raw materials of electrolytic copper (99.99%), pure titanium (99.9%), pure chromium (99.9%) and pure magnesium (99.9%). Table 1 lists the nominal chemical compositions of the investigated Cu−Ti alloys. Cu−4Ti−0.5Cr−0.5Mg, Cu−4Ti−1Cr−0.5Mg, and Cu−4Ti−0.5Cr−1Mg alloy ingots were heated at 900, 850, and 850 °C for 4, 8, and 4 h. The samples were then rapidly quenched in water at room temperature. The solid-solution-treated samples were subjected to hot rolling at a temperature of 830 °C with a total reduction of 70%. After hot rolling, the samples were aged at 450 °C for various durations.

Table 1 Compositions of alloys (wt.%)

Sample	Ti	Cr	Mg	Cu
Cu−4Ti−0.5Cr−0.5Mg	4	0.5	0.5	Bal.
Cu−4Ti−1Cr−0.5Mg	4	1	0.5	Bal.
Cu−4Ti−0.5Cr−1Mg	4	0.5	1	Bal.

The X-ray diffraction (XRD) analysis of the Cu−Ti−Cr−Mg alloys was performed using a Rigaku SmartLab instrument. The scanning angle ranged from 30° to 100° at a scan rate of 8 (°)/min. Microstructural examination of the alloys in their as-cast, solid-solution-treated, and aged states was carried out using an optical microscope (Primotech, ZEISS) and a scanning electron microscope (SEM, TESCAN VEGA 3). Prior to microstructural examination, the samples were polished with 2000 grit sandpaper, followed by mechanical polishing using a diamond polishing paste machine. Subsequently, the samples were etched using a solution of ferric chloride, hydrochloric acid, and anhydrous ethanol. The detailed microstructure during the aging process was observed using a JEOL−2100F transmission electron microscope (TEM), operating at a voltage of 200 kV. Thin slices with a diameter of 3 mm were thinned using a dual-jet electropolishing technique with a chemical solution consisting of 5% nitric acid and 95% methanol. The operating temperature was set to be −30 °C.

The hardness of the samples was measured

using a Vickers hardness tester (HM−102) with a load of 0.5 kg and dwell time of 15 s. To ensure accuracy and reliability, hardness tests were conducted at least five times for each sample and the average values were calculated. The electrical conductivities of the samples were measured using an eddy current conductivity meter (Sigma 2008 B) at 20 °C. Three values were taken for average.

3 Results

3.1 Initial microstructure

Figure 1 shows the initial microstructures of the Cu−4Ti−0.5Cr−0.5Mg, Cu−4Ti−1Cr−0.5Mg, and Cu−4Ti−0.5Cr−1Mg alloys. A typical dendritic structure was observed in all the three samples. The levels of segregation in the as-cast samples varied slightly, depending on the alloying elements. Among the alloys, Cu−4Ti−0.5Cr−1Mg exhibited the smallest dendritic grain size, indicating that the addition of Mg contributed to the refinement of the dendritic crystals.

Figure 2 presents the energy dispersive X-ray spectroscopy (EDS) analysis of the surface elements of the as-cast Cu−4Ti−0.5Cr−0.5Mg, Cu−4Ti−1Cr−0.5Mg, and Cu−4Ti−0.5Cr−1Mg alloys. Local segregation of Cr was observed, while Ti exhibited slight segregation as well.

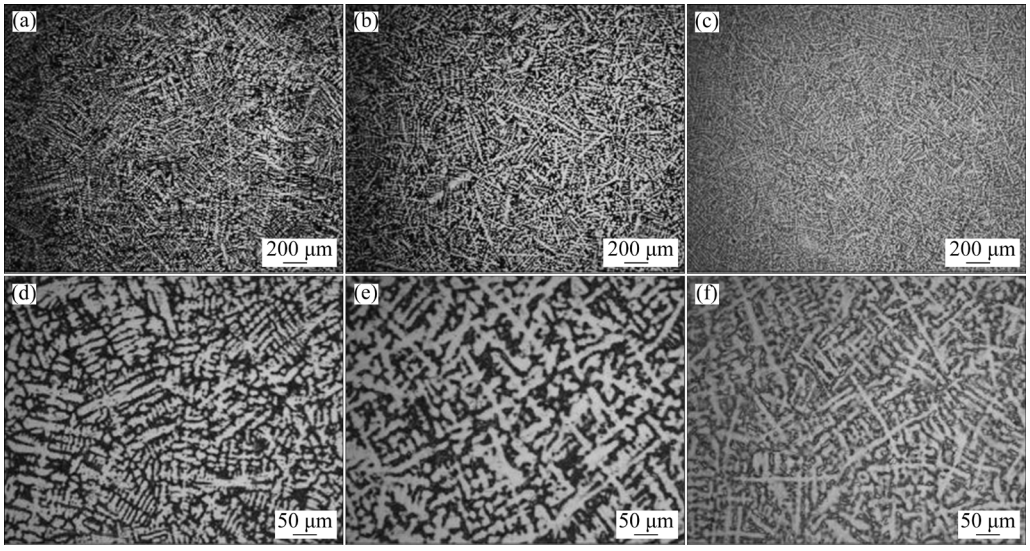

Fig. 1 Microstructures of as-cast alloys: (a, d) Cu−4Ti−0.5Cr−0.5Mg; (b, e) Cu−4Ti−1Cr−0.5Mg; (c, f) Cu−4Ti−0.5Cr−1Mg

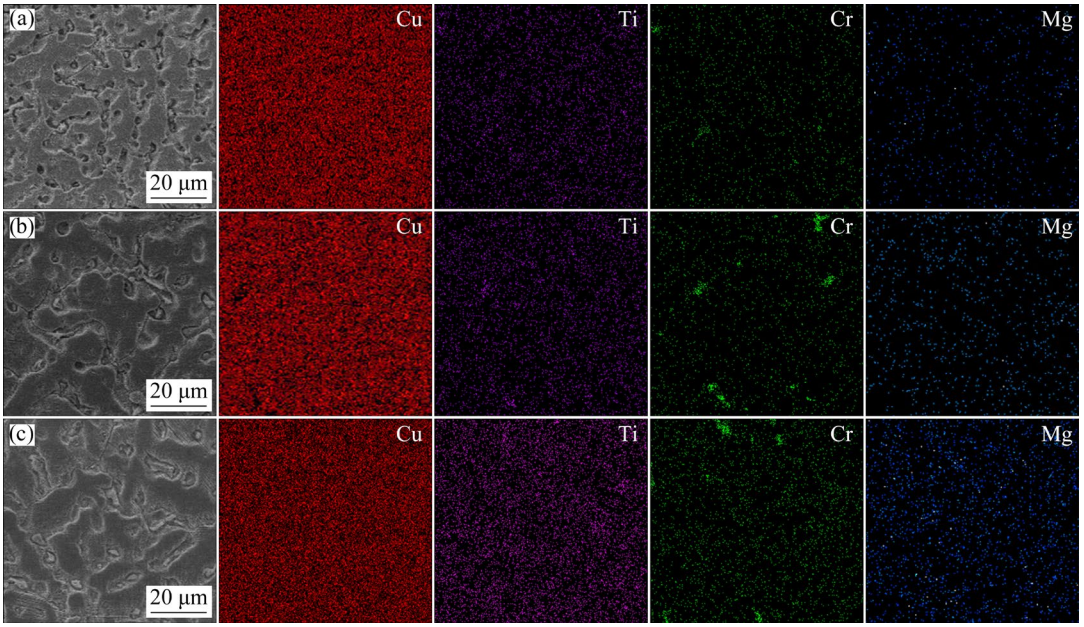

Fig. 2 EDS analysis results of as-cast alloys: (a) Cu−4Ti−0.5Cr−0.5Mg; (b) Cu−4Ti−1Cr−0.5Mg; (c) Cu−4Ti−0.5Cr−1Mg

Figure 3 depicts the microstructure of the Cu−4Ti−0.5Cr−0.5Mg, Cu−4Ti−1Cr−0.5Mg, and Cu−4Ti−0.5Cr−1Mg alloys after the solid-solution treatment. The microstructures of all three alloys after solid-solution treatment exhibited equiaxed grains. The grain size of the Cu−4Ti−0.5Cr−1Mg alloy was significantly refined by Mg addition. Table 2 presents the EDS results of the particles indicated by the yellow arrows in Fig. 3, suggesting that the atomic ratio of Ti to Cr is close to 1:2. This indicated the formation of Cr_2Ti intermetallic compounds. The presence of the Cr_2Ti phase further supports the observation of elemental segregation mentioned earlier.

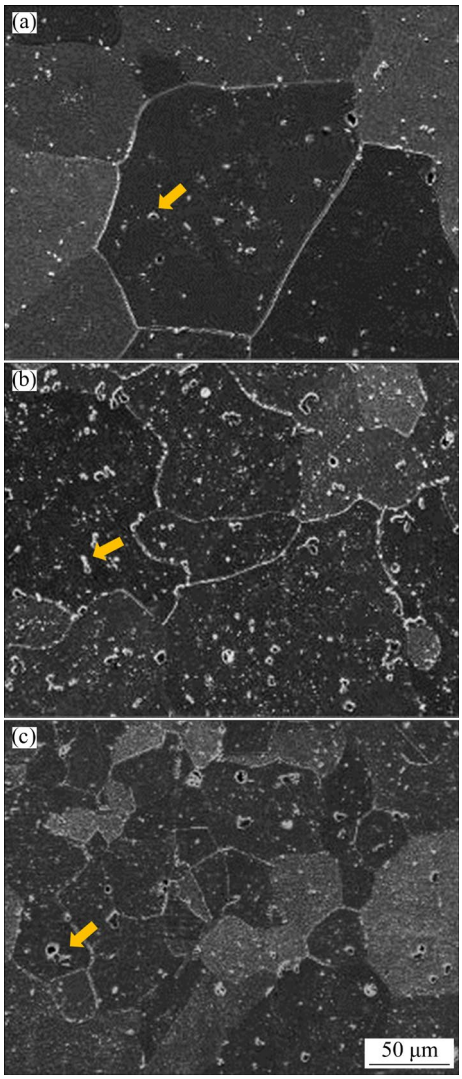

Fig. 3 Microstructures of Cu−4Ti−0.5Cr−0.5Mg after heat treatment at 900 °C for 4 h (a), Cu−4Ti−1Cr−0.5Mg after heat treatment at 850 °C for 8 h (b), and Cu−4Ti−0.5Cr−1Mg alloys after heat treatment at 850 °C for 4 h (c) (The yellow arrows represent Cr_2Ti phases)

Table 2 EDS results taken from yellow arrows shown in Fig. 3 (at.%)

Sample	Cu	Ti	Cr	Mg
Cu−4Ti−0.5Cr−0.5Mg	3.37	31.30	63.59	1.74
Cu−4Ti−1Cr−0.5Mg	3.48	31.67	64.08	0.77
Cu−4Ti−0.5Cr−1Mg	3.76	32.11	63.47	0.66

3.2 Properties

The performance of the alloys after hot rolling and aging was evaluated. The variations in hardness with aging time for the Cu−4Ti−Cr−Mg alloys are illustrated in Fig. 4(a). Observations revealed an initial increase followed by a decrease in the hardness for all three alloys with increasing aging time. After aging for 4 h, peak hardness values of HV 309, 302, and 310 were obtained for the three

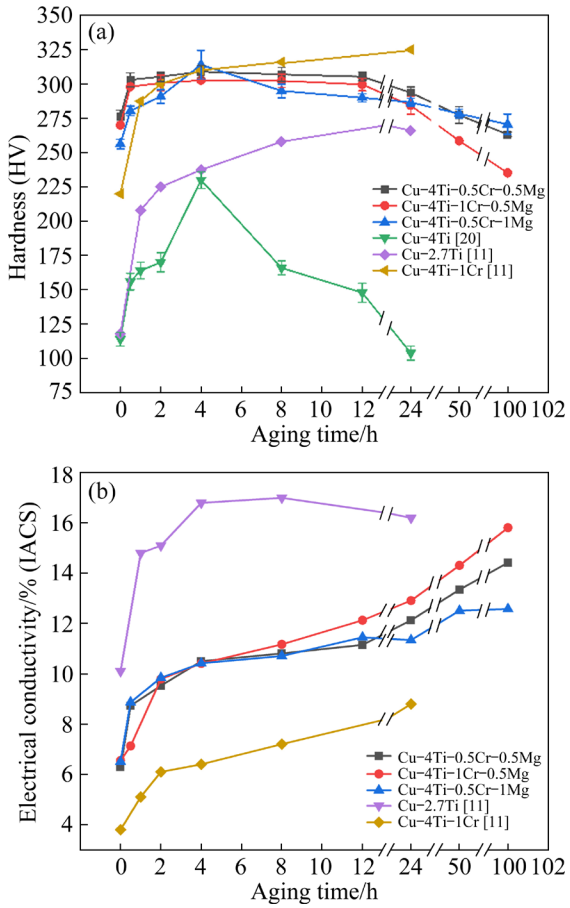

Fig. 4 Hardness variation (a) and electrical conductivity variation (b) of Cu−4Ti−0.5Cr−0.5Mg, Cu−4Ti−1Cr−0.5Mg and Cu−4Ti−0.5Cr−1Mg alloys after aging at 450 °C for different time (The hardness and electrical conductivity data of Cu−4Ti in Ref. [20] and Cu−2.7Ti and Cu−4Ti−1Cr alloys in Ref. [11] are given for comparison)

alloys. Nevertheless, at the over-aged stage, the Cu−4Ti−1Cr−0.5Mg alloy demonstrated the most rapid reduction in hardness, declining to HV 235 after aging for 100 h. On the other hand, the Cu−4Ti−0.5Cr−1Mg alloys exhibited the highest hardness of HV 270 after 100 h of aging.

The binary Cu−4Ti alloy was solid solution treated at 900 °C for 2 h and aged at 500 °C for different durations [20]. The hardness of the Cu−Ti−Cr−Mg alloys in this study was higher than that of a binary Cu−4Ti alloy [20]. This may contribute to the grain boundary strengthening induced by the addition of Cr and Mg elements and hot rolling. The Cu−2.7Ti and Cu−4Ti−1Cr alloys were hot forged, rolled at 850 °C, solution-treated, and aged at 450 °C for different time [11]. The hardness of the Cu−Ti−Cr−Mg alloys in this study is comparable to that of the Cu−4Ti−1Cr alloy. The hardness of Cu−Ti−Cr−Mg alloys is higher than that of Cu−2.7Ti alloy, because of larger Ti contents in the matrix and solute solution strengthening of Cr and Mg elements. The hardness in the present study was rational and higher than that in other studies.

Figure 4(b) shows the variation in electrical conductivity of the Cu−4Ti−0.5Cr−0.5Mg, Cu−4Ti−1Cr−0.5Mg, and Cu−4Ti−0.5Cr−1Mg alloys after aging at 450 °C for different time. The electrical conductivities of all three alloys increased with the aging time. The electrical conductivities of the samples aged for 4 h were 10.5% (IACS), 10.41% (IACS), and 10.42% (IACS). After aging for 100 h, the electrical conductivities of the three alloys were 14.42% (IACS), 15.81% (IACS), and 12.58% (IACS). The electrical conductivity of the Cu−Ti−Cr−Mg alloy in this study was higher than that of the Cu−4Ti−1Cr alloy and lower than that of the Cu−2.7Ti alloy. Figure 4 indicates that the comprehensive performance of the Cu−Ti−Cr−Mg alloys was excellent.

3.3 Analysis of precipitation process

To understand the underlying factors contributing to the performance differences among the three alloys, a detailed analysis of their microstructural characteristics was conducted at various stages: solid solution (SS) treated, early aged (0.5 h), peak-aged (4 h), and over-aged (100 h). XRD analysis was employed to characterize the phase compositions of the three alloys during aging.

The XRD patterns of the three alloys in the solid-solution-treated state and different aging stages at 450 °C are shown in Fig. 5. Notably, the intense diffraction peaks observed for all the alloys were attributed to the presence of the Cu matrix phase. In the solid-solution-treated sample of the Cu−4Ti−0.5Cr−0.5Mg alloy, distinct diffraction peaks associated with the Cr_2Ti phase were identified. The Cr_2Ti phase was distinguished by a

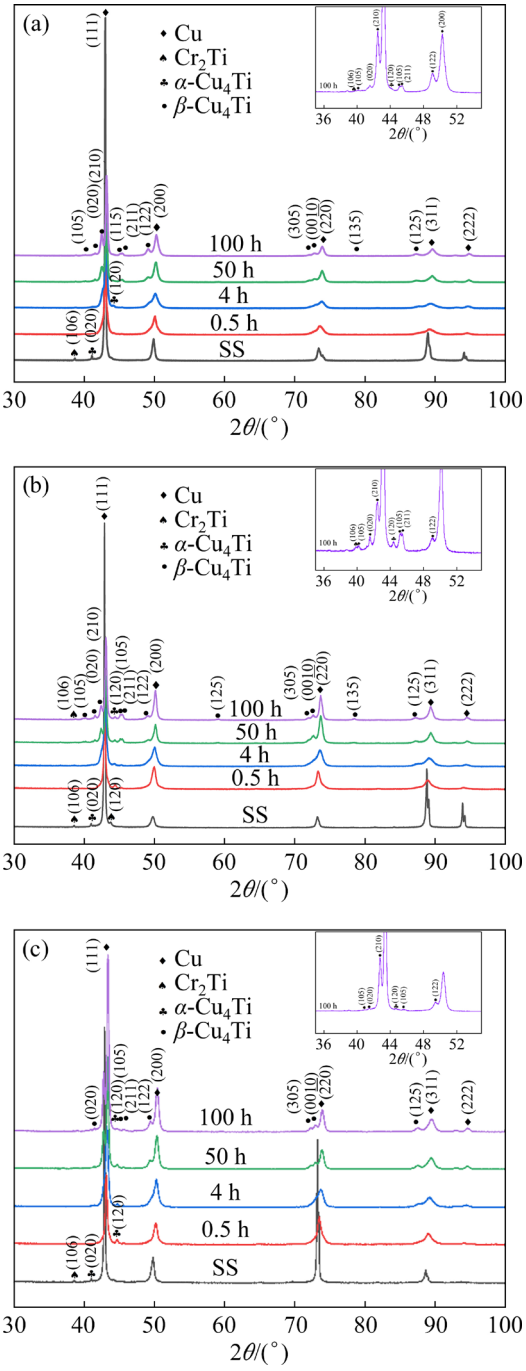

Fig. 5 XRD patterns of Cu−4Ti−0.5Cr−0.5Mg (a), Cu−4Ti−1Cr−0.5Mg (b) and Cu−4Ti−0.5Cr−1Mg (c) alloys at SS-treated state and aged at 450 °C for different durations

face-centered cubic structure with lattice parameters of $a=b=c=$ 0.694 nm. With prolonged aging time, all diffraction peaks originating from the Cu matrix exhibited a progressively higher angular shift. Based on Bragg's law, the larger atomic radius of titanium (2 Å) compared to copper (1.28 Å) causes a reduced interplanar spacing and enlarged diffraction peaks when the titanium content in the matrix is reduced. Consequently, the formation of precipitates causes a rightward deviation of the diffraction peaks with prolonged aging time [21].

After aging for 4 h, it exhibited a metastable phase known as α-Cu_4Ti (also referred to as β'-Cu_4Ti) [22]. The α-Cu_4Ti phase exhibits a tetragonal crystal structure characterized by lattice parameters $a=b$=0.584 nm and c=0.365 nm [23,24]. After aging for 50 h, the content of α-Cu_4Ti phase significantly decreased, whereas a stable phase, referred to as β-Cu_4Ti [4] (alternatively labeled as Cu_3Ti [20]), became predominant. The β-Cu_4Ti precipitates showed an ordered orthorhombic configuration resembling Au_4Zr, with space group of *Pnma* and lattice parameters of a=0.453 nm, b=0.434 nm, and c=1.293 nm. However, there are uncertainties regarding the structure and composition of the stable phase. After 100 h aging, α-Cu_4Ti phase experienced significant depletion, resulting in enhanced prominence of the diffraction peaks associated with the β-Cu_4Ti phase.

Similar to the Cu−4Ti−0.5Cr−0.5Mg alloy, the Cu−4Ti−1Cr−0.5Mg alloy exhibited a similar evolution of Cu matrix peaks during the aging process. After aging for 100 h, the intensity of the diffraction peaks attributed to the β-Cu_4Ti phase in the Cu−4Ti−1Cr−0.5Mg alloy exceeded that of the Cu−4Ti−0.5Cr−0.5Mg alloy. Likewise, the progression of the diffraction peaks arising from the Cu matrix in the Cu−4Ti−0.5Cr−1Mg alloy was consistent with that of the other two alloys. After 100 h of aging, the β-Cu_4Ti phase was observed in the alloy, although with a relatively diminished intensity compared to the other two alloys.

Figure 6 shows SEM images of the Cu−4Ti−0.5Cr−0.5Mg alloy aged at 450 °C for different time. The microstructures of the samples aged at 450 °C for 0, 0.5, and 4 h (Figs. 6(a−c)) prominently displayed equiaxed grain morphology. Distinct precipitates emerged primarily along the grain boundaries in the sample aged at 450 °C for 24 h, as shown in Fig. 6(d). As the aging time increased further, the number of precipitates along the grain boundaries increased, and they began to penetrate the grains, forming a cellular morphology (Figs. 6(e, f)). Yellow arrows represent intermetallic compounds of Cr_2Ti. The Cr_2Ti phase always exists during the aging treatment.

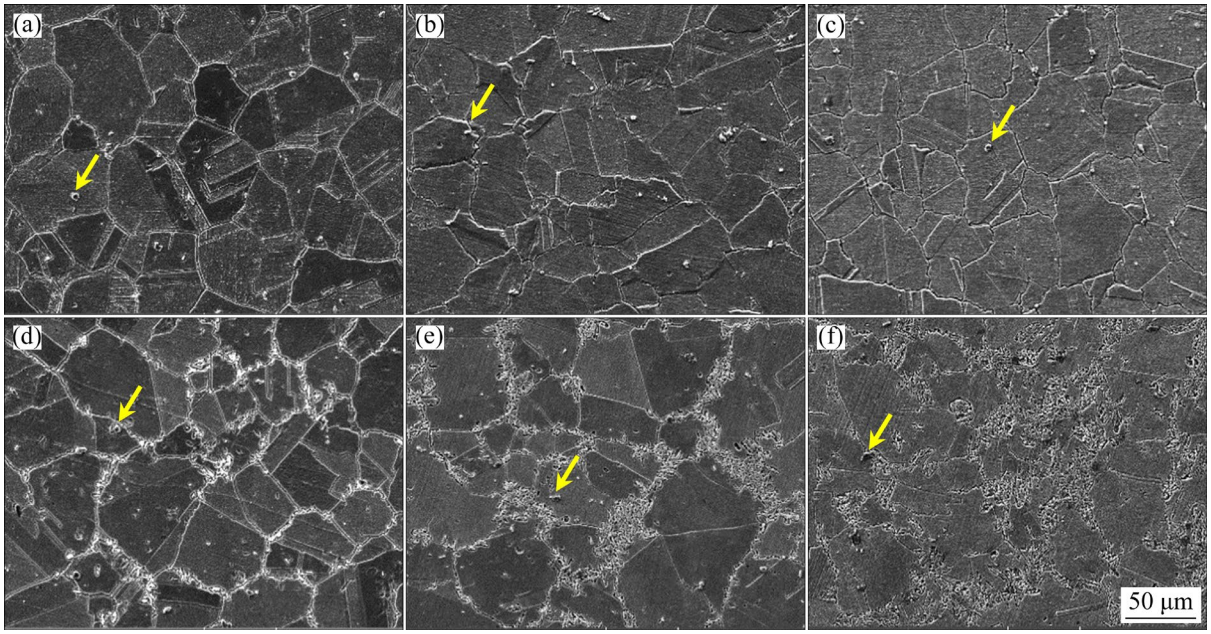

Fig. 6 SEM images of Cu−4Ti−0.5Cr−0.5Mg alloys aged at 450 °C for 0 h (a), 0.5 h (b), 4 h (c), 24 h (d), 50 h (e) and 100 h (f) (Yellow arrows represent intermetallic compounds of Cr_2Ti)

Figure 7 shows SEM images of the Cu−4Ti−1Cr−0.5Mg alloy at different aging time (0, 0.5, 4, 24, 50, and 100 h). No visible precipitates were observed along the grain boundaries during the early stages of aging (Figs. 7(a−c)). However, as the aging time increased to 24, 50, and 100 h, discontinuous precipitates began to form along the grain boundaries. The quantity of these precipitates gradually increased with increasing aging time (Figs. 7(d−f)). Yellow arrows represent intermetallic compounds of Cr_2Ti.

The SEM images in Fig. 8 show the microstructure of the Cu−4Ti−0.5Cr−1Mg alloy at different aging time (0, 0.5, 4, 24, 50, and 100 h). Consistent with the behavior observed in other alloys, no discernible precipitates were detected in the initial stage of aging (Figs. 8(a−c)). However, a limited number of discontinuous precipitates appeared along the grain boundaries after aging at 450 °C for 24 h. Importantly, these precipitates did not exhibit a significant growth in quantity as the aging duration increased (Figs. 8(d−f)). The intermetallic compound of Cr_2Ti is indicated by the yellow arrows.

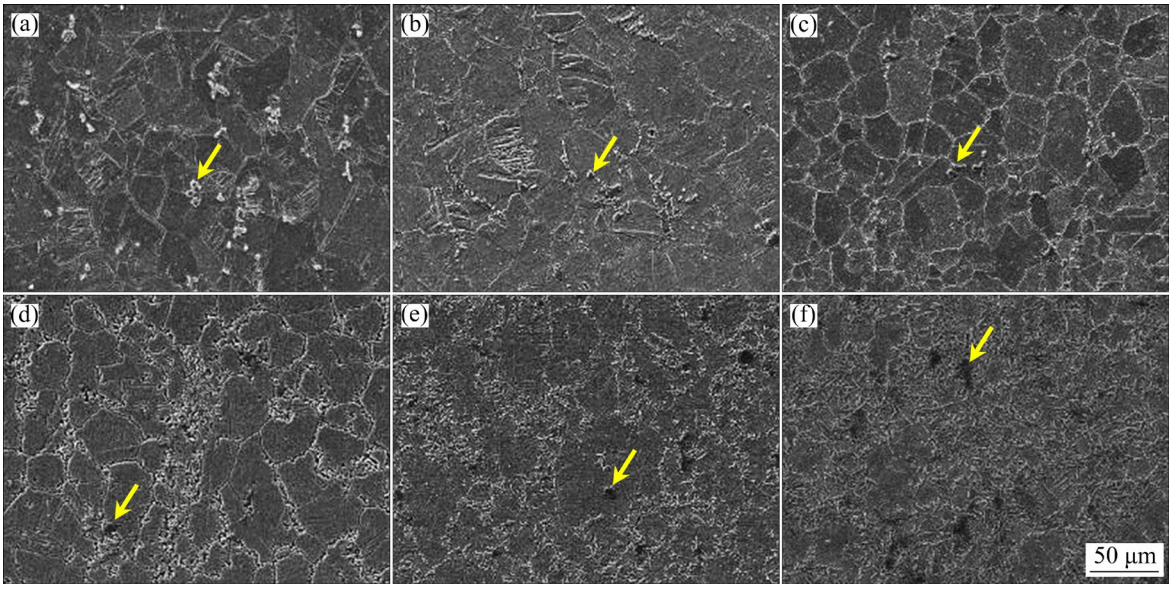

Fig. 7 SEM images of Cu−4Ti−1Cr−0.5Mg alloys aged at 450 °C for 0 h (a), 0.5 h (b), 4 h (c), 24 h (d), 50 h (e) and 100 h (f) (Yellow arrows represent intermetallic compounds of Cr_2Ti)

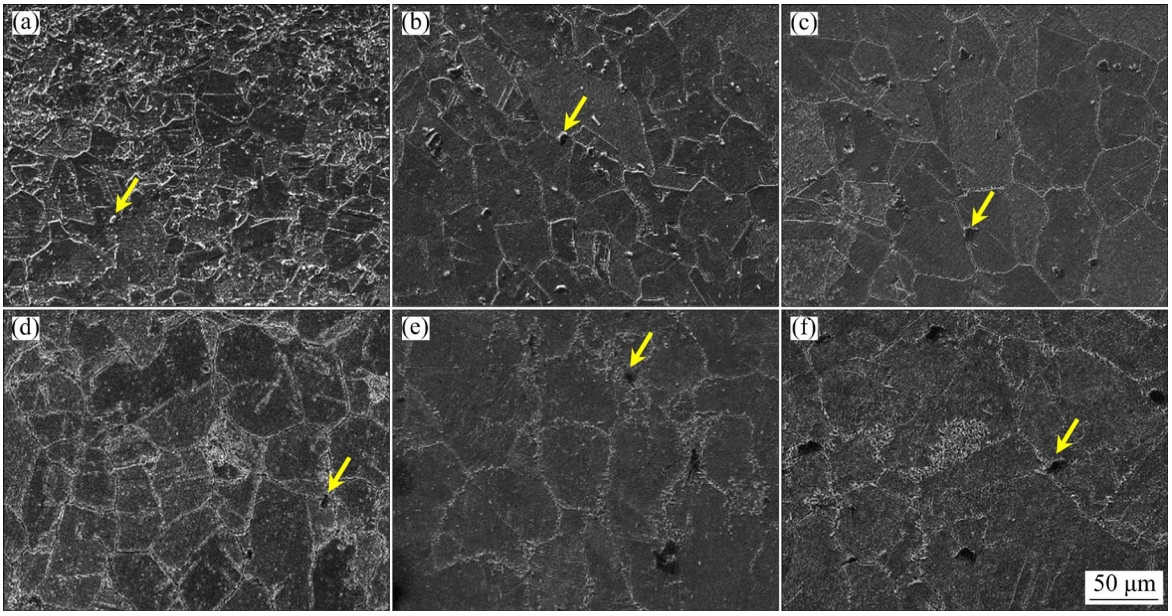

Fig. 8 SEM images of Cu−4Ti−0.5Cr−1Mg alloys aged at 450 °C for 0 h (a), 0.5 h (b), 4 h (c), 24 h (d), 50 h (e) and 100 h (f) (Yellow arrows represent intermetallic compounds of Cr_2Ti)

Figure 9 illustrates microstructural evolution of the Cu−4Ti−0.5Cr−0.5Mg alloy after aging at 450 °C for different time. The TEM image of the specimen aged for 0.5 h (Fig. 9(a)) exhibits distinctive high-contrast undulating patterns and modulated coherent strain characteristics. This is attributed to the decomposition of the initially supersaturated parent α phase into disordered Ti-lean and Ti-rich face-centered cubic particles with sizes on the nanometer scale. This observation is consistent with the images obtained in previous studies on Cu−Ti binary alloys [25]. Selected area electron diffraction (SAED) (inset of Fig. 9(b)) confirmed the formation of ordered metastable precipitates, namely α-Cu_4Ti. These findings are in agreement with results reported in the literature [22,26].

After aging for 4 h (Fig. 9(c)), a uniform dispersion of fine needle-shaped or rod-like α-Cu_4Ti precipitates with lengths of several tens of nanometers was observed within the grain structure. The needle-shaped α-Cu_4Ti precipitates underwent continuous nucleation within the disordered Ti-rich face-centered cubic regions during prolonged aging, eventually attaining maximum lengths of approximately 100 nm, as shown in Fig. 9(c). After aging for 100 h, discontinuous β-Cu_4Ti precipitates with cellular components were formed along the grain boundaries (indicated by the arrows in Fig. 9(d)). Figure 9(e) illustrates the plate-like morphology of the β-Cu_4Ti phase with an orthorhombic crystal structure [27,28]. Plate-like phases aligned along the $\langle 01\bar{1}\rangle_{Cu}$ direction was discernible. Numerous dark and patchy contrast

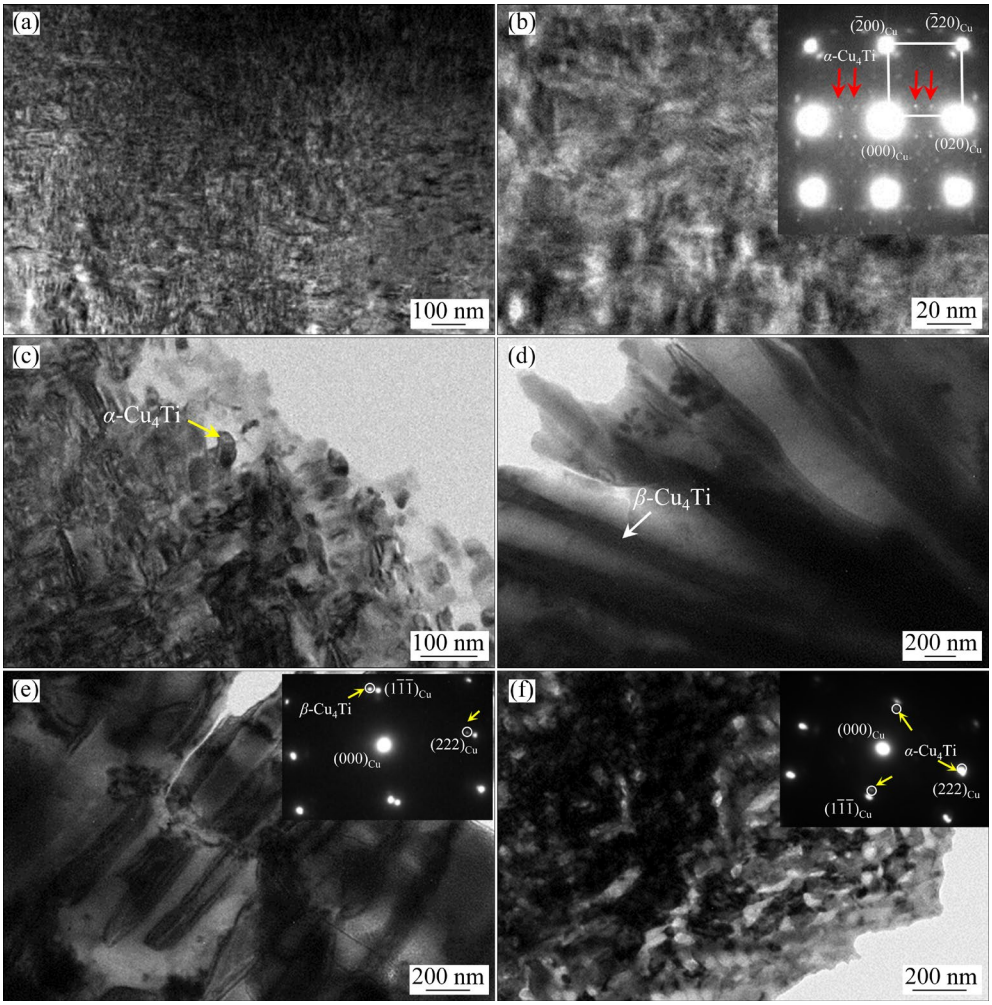

Fig. 9 Bright-field TEM images of Cu−4Ti−0.5Cr−0.5Mg alloys aged at 450 °C for 0.5 h (a, b), 4 h (c) and 100 h (d, e, f) (The insets indicate the corresponding SAED patterns; The red arrows in the SAED pattern of panel (b) indicate the super-lattice reflections from the α-Cu_4Ti phase with a tetragonal structure; The open circles in the SAED pattern of panel (e) are indexed by the β-Cu_4Ti phase; The open circles in the SAED pattern of panel (f) are indexed by the α-Cu_4Ti phase)

features corresponding to the α-Cu_4Ti phase could be observed within the Cu matrix grains. Remarkably, the observed features in Fig. 9(f) resembled those found in the corresponding microstructures of the peak-aged Cu−4Ti alloy [29]. It exhibited identical morphologies to the Cu matrix phase subsequent to over-aging in Cu−Ti alloy [14]. Dual-phase microstructure comprising Cu and α-Cu_4Ti exhibited remarkable stability even during the over-aging period, as evidenced by the expansion of the diffusion paths [30].

TEM image of Cu−4Ti−1Cr−0.5Mg alloy aged at 450 °C for 100 h is presented in Fig. 10. In Fig. 10(a), only the cellular constituents were discernible within the specimen after aging for 100 h. The accompanying SAED pattern illustrated in Fig. 10(b) confirmed that these cellular constituents consisted of a Cu solid solution and β-Cu_4Ti lamellae.

The microstructural evolution of Cu−4Ti−0.5Cr−1Mg alloy specimens during aging at 450 °C is presented in Fig. 11. In Fig. 11(a), the modulated structure was observed. After aging for 4 h, a significant number of nano-sized precipitates were uniformly formed within the supersaturated solid solution, as seen in Fig. 11(b). The results were consistent with the findings documented in Ref. [17]. Notably, certain regions still exhibited the presence of the modulated structure, as indicated by Fig. 11(c). After aging for 100 h, the needle-like or rod-like α-Cu_4Ti phases significantly coarsened, reaching lengths on the order of several hundred nanometers, as illustrated in Fig. 11(d).

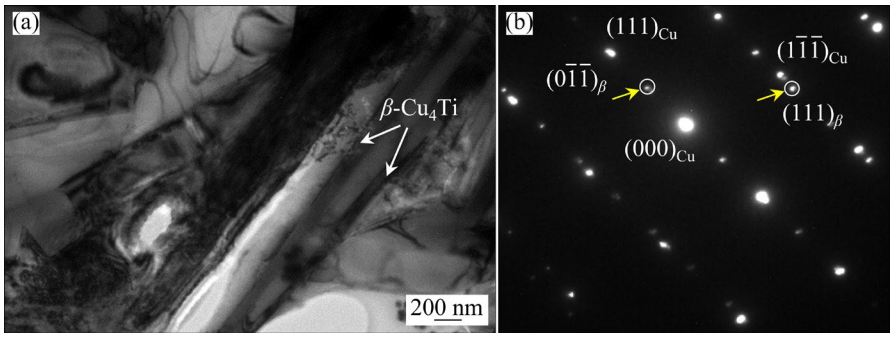

Fig. 10 TEM image (a) and corresponding SAED pattern (b) of Cu−4Ti−1Cr−0.5Mg alloys aged at 450 °C for 100 h (The super-lattice reflections in the SAED pattern of panel (a) are indexed by the β-Cu_4Ti phase with an orthorhombic structure)

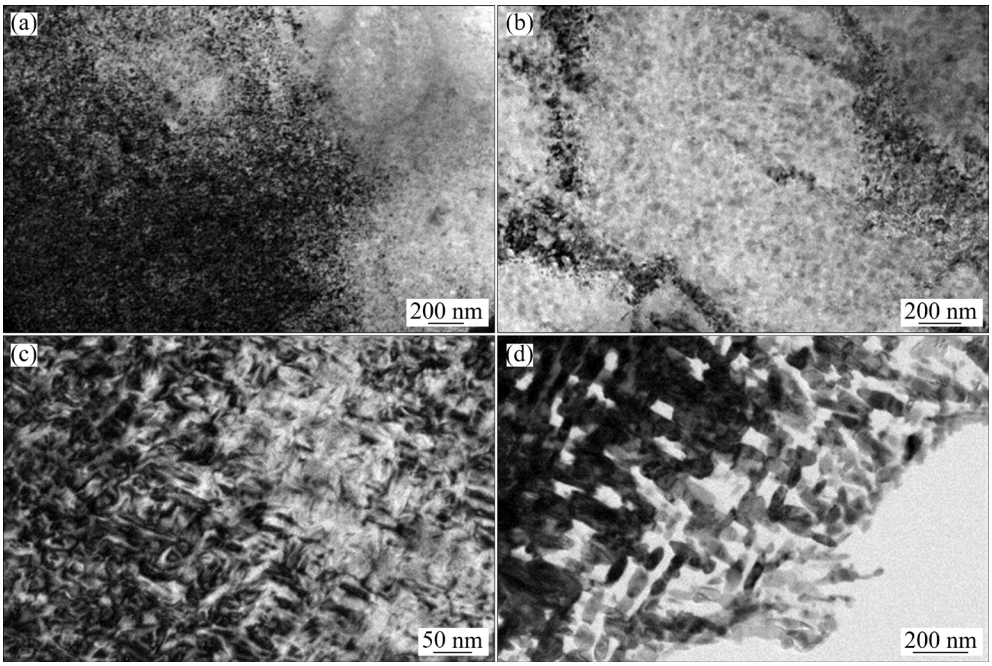

Fig. 11 Bright-field TEM images of Cu−4Ti−0.5Cr−1Mg alloys aged at 450 °C for 0.5 h (a), 4 h (b, c) and 100 h (d)

4 Discussion

4.1 Formation of intermetallic compound Cr_2Ti

Intermetallic compound Cr_2Ti in the Cu−Ti−Cr−Mg alloy was formed during the casting stage, as revealed by the experimental findings. Analysis of the XRD (Fig. 5) and SEM (Figs. 3, 6, 7 and 8) results during solid solution treatment and aging processes revealed the persistence of the Cr_2Ti phase without any changes. The SEM results revealed that the Cr_2Ti particles exhibited an irregular shape, typically with an average width of 2.5 μm. Further insights into the nanoscale characteristics of the irregularly shaped Cr_2Ti particles were provided by TEM observations, indicating an average grain size of 200 nm (Fig. 12). The rod-like Cr_2Ti phase exhibited an average length of 435 nm and an average width of 120 nm, as shown in Fig. 13. The solubility of Cr in Cu was determined to be 1.56 wt.% at elevated temperatures, while Ti in Cu had a solubility of 5.8 wt.%. However, at room temperature, the solubility decreased to less than 0.03 wt.% for Cr and 0.4 wt.% for Ti. Additionally, Cr and Ti exhibited limited solubility in each other below 600 °C, resulting in the formation of the intermetallic phase Cr_2Ti in the system [31]. As noted by HUANG et al [12], the generation of Cr_2Ti particles during the casting process aligned with the findings of this study.

4.2 Effect of Cr and Mg co-addition on microstructure evolution of Cu−Ti alloys

During the initial aging period, the phase transformation process of the Cu−Ti−Cr−Mg alloy exhibits a resemblance to that of the binary Cu−Ti alloy. Moreover, the microstructural characteristics of the three alloys investigated in this study display a fundamental similarity. Modulation decomposition occurs in the supersaturated solid solution and the corresponding microstructure displays distinct high-contrast wavy patterns and modulated coherent strain features (Figs. 9(a) and 11(a)). With increasing aging time, a transition from a short-range to a long-range order takes place. The matrix aged at 450 °C for 4 h exhibits fine-scale α-Cu_4Ti precipitates (Figs. 9(c) and 11(b)), consistent with the previous literature findings [17,30].

Due to the varying content of Cr and Mg elements, significant differences exist in the morphology and quantity of precipitates during the over-aged stage among three Cu−Ti−Cr−Mg

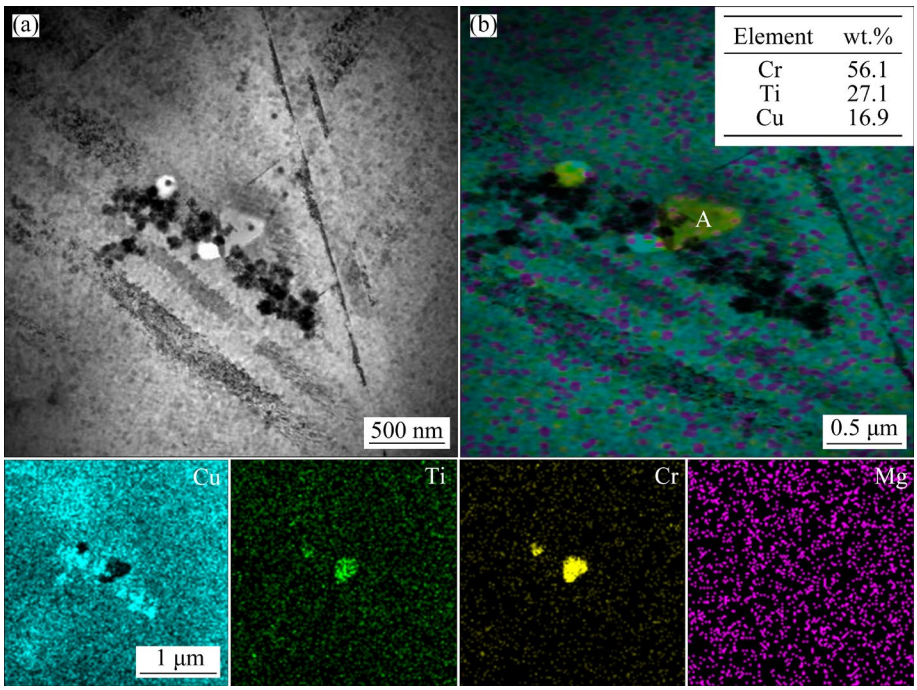

Fig. 12 STEM BF of intermetallic compound particles of Cr_2Ti phase with irregular shape in Cu−4Ti−0.5Cr−0.5Mg alloy aged at 450 °C for 4 h (a); EDS layered image and elements distribution of Cu, Ti, Cr and Mg (b) (The inset in (b) shows EDS results of Point A)

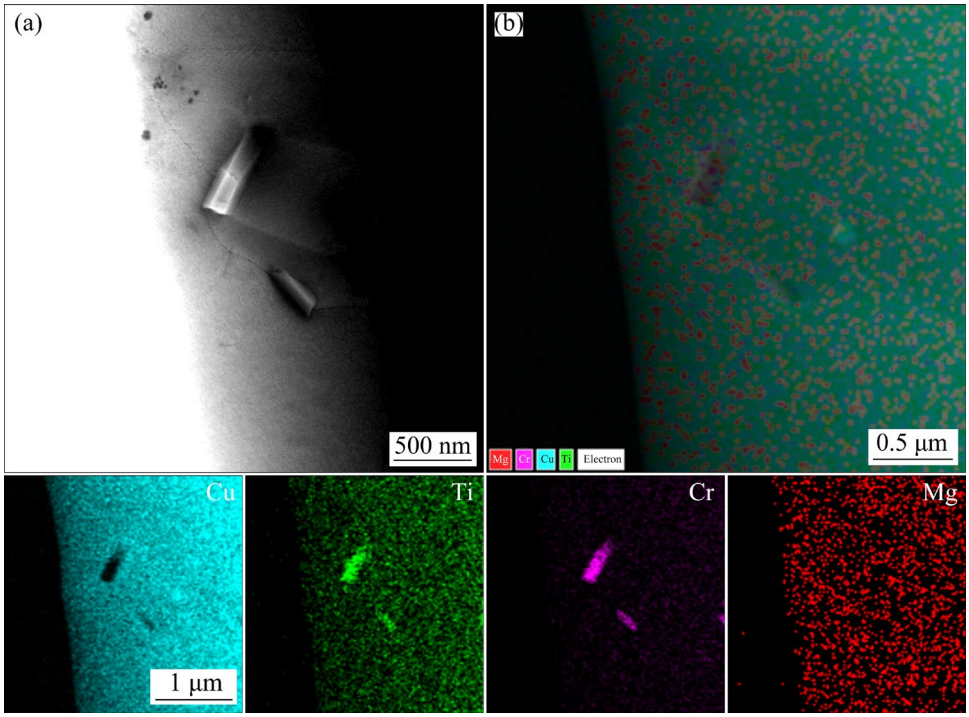

Fig. 13 STEM BF of intermetallic compound particles of rod-like Cr_2Ti phase in Cu−4Ti−0.5Cr−0.5Mg alloy aged at 450 °C for 4 h (a); EDS layered image and elements distribution of Cu, Ti, Cr and Mg (b)

alloys. Both XRD and SEM analyses indicate that after aging for 100 h, the abundance of β-Cu_4Ti precipitates follows the sequence: Cu−4Ti−1Cr−0.5Mg > Cu−4Ti−0.5Cr−0.5Mg > Cu−4Ti−0.5Cr−1Mg. TEM observations reveal that the majority of β-Cu_4Ti precipitates in Cu−4Ti−1Cr−0.5Mg alloy are cellular laminates (Fig. 10). In Cu−4Ti−0.5Cr−0.5Mg alloy, various morphologies can be observed for the β-Cu_4Ti precipitates, including plates and laminates (Figs. 9(d−f)). Compared to Cu−4Ti alloy [32], the Cu−Ti−Cr−Mg alloys investigated in this study effectively suppress the formation of discontinuous precipitates.

The Cu−4Ti−0.5Cr−1Mg alloy demonstrates the precipitation of nanoscale square-shaped α-Cu_4Ti phase after aging for 4 h (Fig. 11(b)). Both the Cu−4Ti−0.5Cr−0.5Mg and Cu−4Ti−0.5Cr−1Mg alloys aged for 100 h retain the α-Cu_4Ti precipitates within the Cu matrix, displaying a rod-like morphology similar to that observed during peak aging in binary alloys [30]. The bright-field TEM image was utilized to measure the average length and width of the precipitated phase. To determine the size of the precipitated phases along different directions, the average value was calculated from data obtained from five images captured in various areas at the same aging time.

The α-Cu_4Ti phase in the Cu−4Ti−0.5Cr−0.5Mg alloy exhibits an average width of 46 nm and an average length of 67 nm. Within the Cu−4Ti−0.5Cr−1Mg alloy, the α-Cu_4Ti phase demonstrates an average width of 37 nm and an average length of 84 nm. The Ostwald ripening law governs the growth rate of the α-Cu_4Ti precipitates with increasing aging time [12]. According to previous studies [33], discontinuous precipitates are known to initiate nucleation at grain boundaries, with their growth being accompanied by grain boundary migration. A comparison between the Cu−4Ti−0.5Cr−0.5Mg and Cu−4Ti−1Cr−0.5Mg alloys reveals that an elevated Cr content results in an increased occurrence of β-Cu_4Ti precipitates along the grain boundaries. However, these findings contradict the outcomes obtained from the Cu−3Ti−1Cr alloy [12]. The discrepancy can be attributed to the presence of nano-sized Cr phases within the Cu−3Ti−1Cr alloy, which occupy the nucleation sites of discontinuous precipitates at these grain boundaries. Thereby they impede the formation of β-Cu_4Ti precipitates. In contrast, the investigated Cu−Ti−Cr−Mg alloys in this study do not exhibit the existence of nano-sized Cr phases.

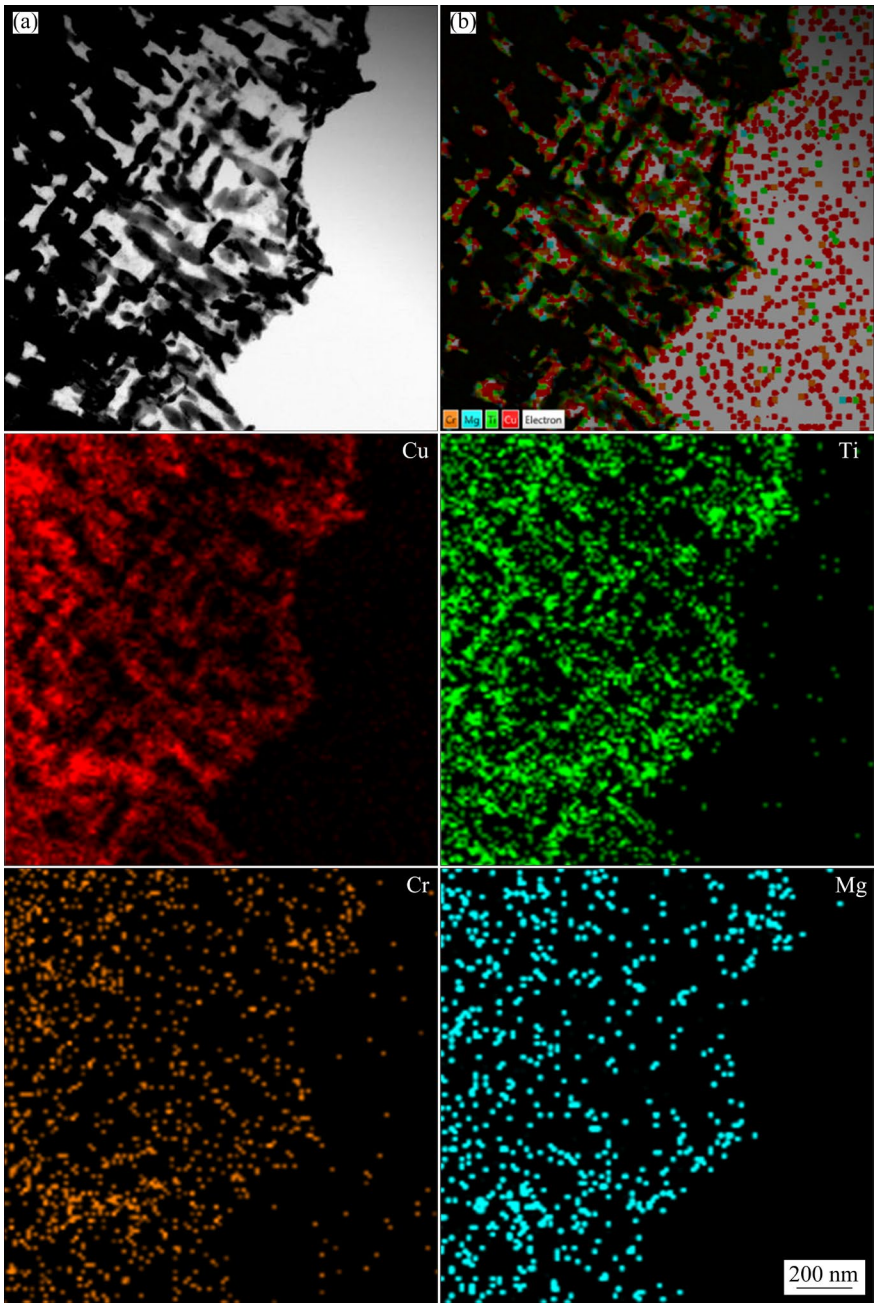

Fig. 14 STEM BF of Cu−4Ti−0.5Cr−0.5Mg alloy aged at 450 °C for 100 h (a); EDS layered image and elements distribution of Cu, Ti, Cr and Mg (b)

By comparing the Cu−4Ti−0.5Cr−0.5Mg and Cu−4Ti−0.5Cr−1Mg alloys, it is observed that an increased Mg content correlates with a decrease in the number of discontinuous precipitates along the grain boundaries. This phenomenon can be explained by the chemical characteristics of Mg, as it neither reacts with Cr nor dissolves in it [34]. Consequently, Mg atoms are expelled from the precipitates during the aging process [35]. Moreover, the diffusion of Mg atoms in Cu occurs at a slower rate compared to Cr atoms, mainly attributed to the increased solubility of Mg in Cu [14]. Consequently, the accelerated diffusion of Mg atoms from the precipitates results in their accumulation at the precipitate/matrix interface, leading to the formation of segregation.

Additionally, the incorporation of Mg atoms into vacancies reduces the elastic misfit energy between the matrix and precipitates, thereby releasing distortional strain energy and ultimately diminishing the driving force for competitive coarsening [35]. Furthermore, the presence of

enriched Mg along the precipitate/matrix interface creates a conducive environment that effectively immobilizes the interface [36], as illustrated in Fig. 14. Figure 15 provides an enlarged depiction of Fig. 14, showing the simultaneous existence of continuous precipitates ranging from several hundred nanometers to a few nanometers in size. By synergistically leveraging the effects of Mg discussed earlier, the incorporation of Mg into Cu−Ti alloys significantly reduces the coarsening rate of continuous precipitates and effectively inhibits the formation of discontinuous precipitates.

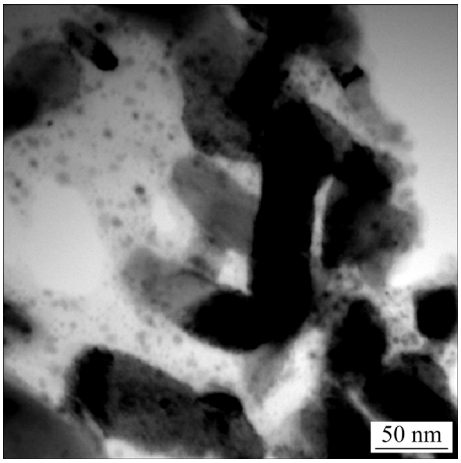

Fig. 15 STEM BF of Cu−4Ti−0.5Cr−0.5Mg alloy aged at 450 °C for 100 h, showing nanoscale α-Cu_4Ti precipitates

4.3 Effect of Cr and Mg co-addition on properties of Cu−Ti alloys

The incorporation of Cr and Mg has a considerable impact on the performance of Cu−Ti alloys. The Cu−4Ti−0.5Cr−1Mg alloy displayed superior hardness after aging for 4 h. The most significant increment of hardness was observed from 2 to 4 h. This phenomenon can be ascribed to the acceleration of precipitation nucleation by Mg (Fig. 11) and the refinement of grain sizes (Fig. 3) [37]. Furthermore, the influence of Mg becomes more pronounced during the over-aged stage, specifically between 4 and 8 h, when the Cu−4Ti−0.5Cr−1Mg alloy exhibits the most substantial decrease in hardness. This is mainly because the increase in Mg content effectively inhibits the formation of β-Cu_4Ti discontinuous precipitates and reduces the coarsening of α-Cu_4Ti continuous precipitates.

According to Mathiessen's law [38,39], the presence of solid solution atoms is the primary factor contributing to the increase in resistance observed in alloys. Different alloying elements have varying effects on the electrical conductivity of copper alloys. It was found that Ti had the most significant influence, followed by Cr, whereas the influence of Mg remained minimal [40]. The Cu matrix of the three alloys underwent EDS point scanning analysis at different aging stages, as illustrated in Fig. 16. In the solid solution state, the electrical conductivity followed the sequence: Cu−4Ti−0.5Cr−0.5Mg > Cu−4Ti−1Cr−0.5Mg > Cu−4Ti−0.5Cr−1Mg. The difference in Ti content

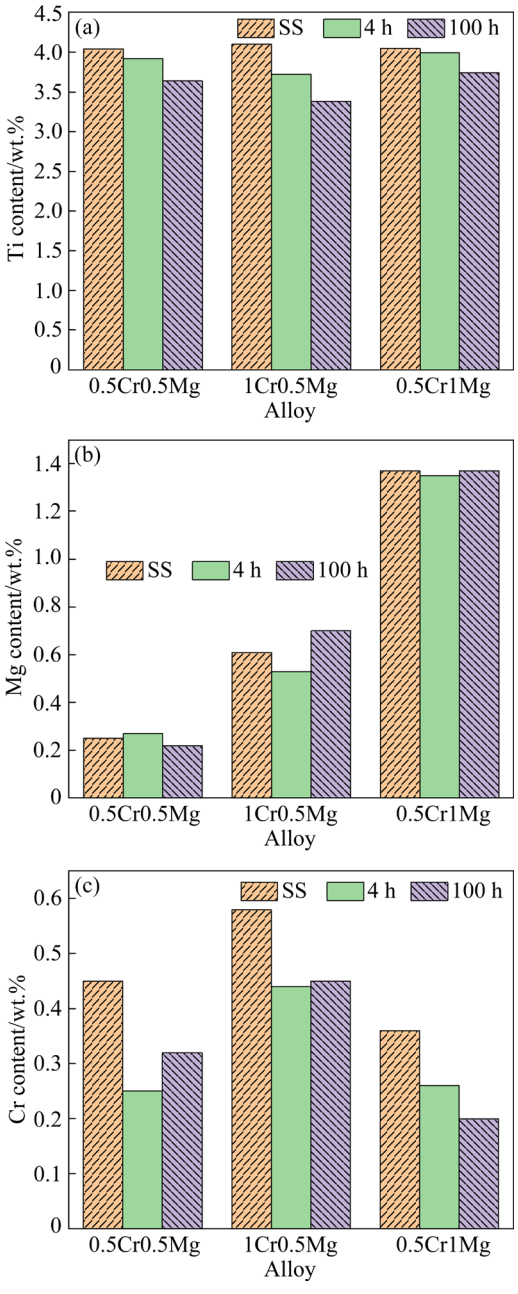

Fig. 16 EDS results obtained from Cu matrix in Cu−Ti−Cr−Mg alloys aged for different time: (a) Ti content; (b) Mg content; (c) Cr content

among the three alloys in the solid solution state is negligible. The Cu−4Ti−1Cr−0.5Mg alloy, possessing the highest concentration of solid solution Cr, manifests the lowest electrical conductivity.

During the aging process, particularly at the peak-aged stage, the electrical conductivity of the three alloys remained nearly indistinguishable, due to the basically equal solid solution Ti contents. However, when the aging time extended to 100 h, the Cu−4Ti−0.5Cr−1Mg alloy displayed the smallest amount of precipitates and the highest concentration of the solid solution Ti atoms. Consequently, Cu−4Ti−0.5Cr−1Mg alloy exhibited the lowest electrical conductivity, which was attributed to the combined influence of Mg and Cr elements.

5 Conclusions

(1) The microstructure of three Cu−Ti−Cr−Mg alloys consisted of Cr_2Ti, α-Cu_4Ti and Cu phases in solid-solution-treated state. In the early-aged stage, the initially supersaturated parent α phase decomposed into disordered Ti-lean and Ti-rich particles. Then, nanoscale α-Cu_4Ti continuous precipitates were formed in the peak-aged stage. Subsequently, α-Cu_4Ti precipitates coarsened, and β-Cu_4Ti discontinuous precipitates appeared.

(2) The co-addition of Cr and Mg elements increased the hardness of Cu−Ti alloys compared to binary Cu−Ti alloys. The Cu−4Ti−0.5Cr−0.5Mg, Cu−4Ti−1Cr−0.5Mg, and Cu−4Ti−0.5Cr−1Mg alloys displayed peak hardness values of HV 309, 302, and 310, respectively.

(3) Co-addition of Cr and Mg elements effectively suppressed the formation of β-Cu_4Ti precipitates during the over-aged stage. As the Mg content increased in the Cu−Ti−Cr−Mg alloy, both the growth rate of α-Cu_4Ti precipitates and the quantity of β-Cu_4Ti precipitates decreased after aging at 450 °C for 100 h.

(4) Mg atoms uniformly distributed in the copper matrix in the solid solution treatment. During the aging process, Mg accumulated at the precipitate/matrix interface, leading to the formation of segregation. This phenomenon released distortional strain energy and ultimately diminished the driving force for competitive coarsening.

CRediT authorship contribution statement

Huan WEI: Investigation, Methodology, Formal analysis, Writing − Original draft, Funding acquisition; **Hong-li WEI:** Investigation; **Hua-yun DU:** Writing − Review & editing; **Qian WANG:** Writing – Review & editing; **Cai-zhi ZHOU:** Writing – Review & editing; **Ying-hui WEI:** Supervision, Writing − Reviewing & editing; **Li-feng HOU:** Writing – Review & editing, Funding acquisition.

Declaration of competing interest

The authors declare that they have no known competing financial interests or personal relationships that could have appeared to influence the work reported in this paper.

Acknowledgments

This work was supported by the National Natural Science Foundation of China (No. 52201226), Fundamental Research Program of Shanxi Province, China (No. 202103021223036), the Key Scientific Research Project in Shanxi Province, China (No. 202102050201007), and the special fund for Science and Technology Innovation Teams of Shanxi Province, China (No. 202204051001004).

References

[1] QIN Liu-xin, ZHOU Tao, JIANG Xiao-yu, WANG Meng, HU Jin-hui, WU Zi-xiao, MENG Xiang-peng, JIANG Yan-bin, LI Zhou. Microstructure and properties of Cu−Ni−Co−Si−Cr−Mg alloy by multistage thermo-mechanical treatment [J]. Transactions of Nonferrous Metals Society of China, 2023, 23(12): 3739−3755. https://doi.org/10.1016/S1003-6326(23)66367-8.

[2] ZHANG Hong-tao, JIANG Yan-bin, XIE Jian-xin, LI Yong-hua, YUE Li-juan. Precipitation behavior, microstructure and properties of aged Cu−1.7wt.%Be alloy [J]. Journal of Alloys and Compounds, 2019, 773(30): 1121−1130. https://doi.org/10.1016/j.jallcom.2018.09.296.

[3] HUANG Xia-xu, XIE Guo-liang, LIU Xin-hua, FU Hua-dong, SHAO Lei, HAO Zi-fan. The influence of precipitation transformation on Young's modulus and strengthening mechanism of a Cu−Be binary alloy [J]. Materials Science and Engineering A, 2020, 772: 138592. https://doi.org/10.1016/j.msea.2019.138592.

[4] TU Ying-ming, LIU Xue-feng, WANG Wen-jing, ZHANG Wei-liang, FENG Qi-hang. Deformation-aging behavior and property evolution of Cu−Ti alloys prepared by accumulative roll bonding-deformation diffusion process [J]. Materials Science and Engineering A, 2022, 855: 143915. https://doi.org/10.1016/j.msea.2022.143915.

[5] YANG Hai-te, WANG Wen-wei-jiao, WANG Chen, WANG jian, ZHOU Jian-hui, TONG Chang-qing, CHEN Jun-feng, WANG Bing-shu. Effect of aging process on properties and precipitation kinetics of Cu−Cr−Zr alloy strips [J].

Transactions of Nonferrous Metals Society of China, 2023, 33(8): 2439−2448. https://doi.org/10.1016/S1003-6326(23)66271-5.

[6] XIN Gang-ao, ZHOU Meng, JING Ke, HU Hao-yan, LI Zheng-ao, ZHANG Yi, BAI Qian, TIAN Cai-jiao, TIAN Bao-hong, LI Xu, VOLINSKY A A, ZOU Jin. Heat treatment effects on microstructure and properties of Cu−Ti−Fe alloys [J]. Materials Science and Engineering A, 2024, 892: 146068. https://doi.org/10.1016/j.msea.2023.146068.

[7] KONNO T J, NISHIO R, SEMBOSHI S, OHSUNA T, OKUNISHI E. Aging behavior of Cu−Ti−Al alloy observed by transmission electron microscopy [J]. Journal of Materials Science, 2008, 43(11): 3761−3768. https://doi.10.1007/s10853-007-2233-2.

[8] NAGARJUNA S, SHARMA K K, SUDHAKAR I, SARMA D S. Age hardening studies in a Cu−4.5Ti−0.5Co alloy [J]. Materials Science and Engineering A, 2001, 313: 251−260. https://doi.org/10.1016/S0921-5093(00)01834-7.

[9] LIU Jia, WANG Xian-hui, RAN Qian-ni, ZHAO Gang, ZHU Xiu-xiu. Microstructure and properties of Cu−3Ti−1Ni alloy with aging process [J]. Transactions of Nonferrous Metals Society of China, 2016, 26(12): 3183−3188. https://doi.org/10.1016/S1003-6326(16)64450-3.

[10] LIU Jia, WANG Xian-hui, GUO Ting-ting, ZHOU Jun-tao, YANG Xiao-hong. Microstructural evolution and properties of aged Cu−3Ti−3Ni alloy [J]. Rare Metal Materials and Engineering, 2016, 45(5): 1162−1167. https://doi.org/10.1016/S1875-5372(16)30113-8.

[11] MARKANDEYAS R, NAGARJUNAD S, SARMA D S. Precipitation hardening of Cu−Ti−Cr alloys [J]. Materials Science and Engineering A, 2004, 371: 291−305. https://doi.org/10.1016/j.msea.2003.12.002.

[12] HUANG Lue, PENG Li-jun, MI Xu-jun, ZHAO Gang, HUANG Guo-jie, XIE Hao-feng, ZHANG Wen-jing. Relationship between microstructure and properties of high-strength Cu−Ti−Cr alloys during aging [J]. Journal of Alloys and Compounds, 2023, 942: 168865. https://doi.10.1016/j.jallcom.2023.168865.

[13] LIU Jia, WANG Xian-hui, RAN Qian-ni , LIU Yan-feng, LI Cong. Pre-deformation and aging characteristics of Cu−3Ti−2Mg alloy [J]. Rare Metal Materials and Engineering, 2018, 47(7): 1980−1985. https://doi.org/10.1016/S1875-5372(18)30168-1.

[14] SAITO K, SUZUKI M, HAYASAKA Y, TAKENAKA K, SEMBOSHI S. Effect of magnesium doping on discontinuous precipitation in age-hardenable copper–titanium alloys [J]. Materials Characterization, 2022, 189: 111911. https://doi.org/10.1016/j.matchar.2022.111911.

[15] LIU Jia, WANG Xian-hui, CHEN Jian, LIU Ji-tuo. The effect of cold rolling on age hardening of Cu−3Ti−3Ni−0.5Si alloy [J]. Journal of Alloys and Compounds, 2019, 797: 370−379. https://doi.org/10.1016/j.jallcom.2019.05.091.

[16] LI Si, LI Zhou, XIAO Zhu, LI San-hua, SHEN Lei-nuo, DONG Qi-yi. Microstructure and property of Cu−2.7Ti−0.15Mg−0.1Ce−0.1Zr alloy treated with a combined aging process [J]. Materials Science and Engineering A, 2016, 650: 345−353. https://doi.org/10.1016/j.msea.2015.10.062.

[17] WANG Xu, XIAO Zhu, QIU Wen-ting, LI Zhou, LIU Feng. The evolution of microstructure and properties of a Cu−Ti−Cr−Mg−Si alloy with high strength during the multi-stage thermomechanical treatment [J]. Materials Science and Engineering A, 2021, 803: 140510. https://doi.org/10.1016/j.msea.2020.140510.

[18] HUANG Lan, CUI Zhen-shan, MENG Xiang-peng, ZHANG Xian-wei, ZHANG Xiao-yan, SONG Xi-ping, TANG Ning, XIAO Zhu, LEI Qian, LI Zhou. Effects of microelements on the microstructure evolution and properties of ultrahigh strength Cu−Ti alloys [J]. Materials Science and Engineering A, 2021, 823: 141581. https://doi.org/10.1016/j.msea.2021.141581.

[19] WANG Xu, XIAO Zhu, MENG Xiang-peng, YI Yu-hang, CHEN Lei. Microstructure and properties evolution of Cu−Ti−Cr−Mg alloy during equal channel angular pressing at room temperature and cryogenic temperature [J]. Journal of Alloys and Compounds, 2022, 927: 166940. https://doi.org/10.1016/j.jallcom.2022.166940.

[20] WEI Huan, WEI Ying-hui, HOU Li-feng, DANG Ning. Correlation of ageing precipitates with the corrosion behaviour of Cu−4wt.%Ti alloys in 3.5 wt.% NaCl solution [J]. Corrosion Science, 2016, 111: 382−390. https://doi.org/10.1016/j.corsci.2016.05.029.

[21] WEI Huan, DAI Xin-yu, HAN Peng-ju, ZHOU Cai-zhi, WEI Ying-hui, HOU Li-feng. Surface mechanical attrition treatment-induced dissolution of Cu_4Ti precipitates in Cu−4wt.%Ti alloy [J]. Materials Science and Technology, 2020, 36(1): 1−7. https://doi.org/10.1080/02670836.2020.1726600.

[22] SEMBOSHI S, AMANO S, FU J, IWASE A, TAKASUGI T. Kinetics and equilibrium of age-induced precipitation in Cu−4 At. Pct Ti binary alloy [J]. Metallurgical and Materials Transactions A, 2017, 48(3): 1501−1511. https://doi.10.1007/s11661-016-3949-x.

[23] HUANG Lue, PENG Li-jun, LI Jiang, MI Xu-jun, ZHAO Gang, XIE Hao-feng, ZHANG Wen-jing, YUAN He-feng, YANG Zhen. Crystallography and diffraction patterns of the precipitates in Cu−3wt.%Ti alloy [J]. Journal of Materials Research and Technology, 2023, 25: 6503−6510. https://doi.org/10.1016/j.jmrt.2023.07.072.

[24] LIAO Yu-min, GUO Cheng-jun, ZHOU Chen-yang, XIE Wei-bin, YANG Bin, WANG Hang. Stability of the metastable β'-Cu_4Ti phase in CuTi alloys: Role of the Ti content [J]. Materials Characterization, 2023, 203: 113164. https://doi.10.1016/j.matchar.2023.113164.

[25] WANG Xu, DING Yan-jun, JIANG Xin-feng, MENG Xiang-peng, XIAO Zhu. Effects of Fe content on properties and microstructure of Cu−Ti alloys during aging [J]. Journal of Materials Research and Technology, 2023, 27: 5518−5532. https://doi.org/10.1016/j.jmrt.2023.10.211.

[26] FU Yi-lei, XIE Guo-liang, ZHAO Fan, WAN Jin-feng, MENG Xiang-hao, LIU Xiao, WANG Rui, LIU Xin-hua. Precipitation behaviors and property variations of Cu−3.0wt.%Ti fabricated by a novel short-processing non-vacuum heating-cooling combined mold continuous casting [J]. Journal of Alloys and Compounds, 2022, 921: 166059. https://doi.org/10.1016/j.jallcom.2022.166059.

[27] ZHU Y D, YAN M F, ZHANG Y X, ZHANG C S. First-principles investigation of structural, mechanical and electronic properties for Cu−Ti intermetallics [J].

Computational Materials Science, 2016, 123: 70−78. https://doi.org/10.1016/j.commatsci.2016.06.015.

[28] CHEN Shuai, DUAN Yong-hua, HUANG Bo, HU Wen-cheng. Structural properties, phase stability, elastic properties and electronic structures of Cu−Ti intermetallics [J]. Philosophical Magazine, 2015, 95(32): 1−19. https://doi.org/10.1080/14786435.2015.1091110.

[29] SAITO K, SUZUKI M, SEMBOSHI S, SATO K, HAYASAKA Y. Isothermal aging behaviors of copper–titanium–magnesium supersaturated solid-solution alloys [J]. Materials Transactions, 2020, 61(10): 1912−1921. https://doi.org/10.2320/matertrans.MT-M2020149.

[30] SOFFA W A, LAUGHLIN D E. High-strength age hardening copper–titanium alloys: Redivivus [J]. Progress in Materials Science, 2004, 49(3): 347−366. https://doi.org/10.1016/S0079-6425(03)00029-X.

[31] MARKANDEYA R, NAGARJUNA S, SARMA D S. Precipitation hardening of Cu−Ti−Cr alloys [J]. Materials Science and Engineering A, 2004, 371: 291−305. https://doi.10.1016/j.msea.2003.12.002.

[32] WEI Huan, CUI Yan-chao, CUI Hui-qi, ZHOU Cai-zhi, HOU Li-feng, WEI Ying-hui. Evolution of grain refinement mechanism in Cu−4wt.%Ti alloy during surface mechanical attrition treatment [J]. Journal of Alloys and Compounds, 2018, 763: 835−843. https://doi.org/10.1016/j.jallcom.2018.06.043.

[33] LI Zhi-qiang, WANG Jun-sheng, HUANG Hou-bing. Influences of grain/particle interfacial energies on second-phase particle pinning grain coarsening of polycrystalline [J]. Journal of Alloys and Compounds, 2019, 818: 152848. https://doi.org/10.1016/j.jallcom.2019.152848.

[34] MOFFATT W. The handbook of binary phase diagrams [M]// Physics: Materials Science. New York: General Electric Co., 1984.

[35] JIANG Su-he, WANG Hui, WU Yuan, LIU Xiong-jun, CHEN Hong-hong, YAO Meng-ji, GAULT B, PONGE D, RAABE D, HIRATA A, CHEN Ming-wei, WANG Yan-dong, LU Zhao-ping. Ultrastrong steel via minimal lattice misfit and high-density nanoprecipitation [J]. Nature, 2017, 544(7651): 460−464. https://doi.0.1038/nature22032.

[36] TANG F, GIANOLA D S, MOODY M P, HEMKER K J, CAIRNEY J M. Observations of grain boundary impurities in nanocrystalline Al and their influence on microstructural stability and mechanical behaviour [J]. Acta Materialia, 2012, 60(3): 1038−1047. https://doi.org/10.1016/j.actamat.2011.10.061.

[37] ZHAO Zi-qian, XIAO Zhu, LI Zhou, MA Mu-zhi, DAI Jie. Effect of magnesium on microstructure and properties of Cu−Cr alloy [J]. Journal of Alloys and Compounds, 2018, 752: 191−197. https://doi.org/10.1016/j.jallcom.2018.04.159.

[38] LENGELER B, SCHILLINGH W, WENZL H. Deviations from Matthiessen's rule and longitudinal magnetoresistance in cold-worked and neutron-irradiated copper [J]. Journal of Low Temperature Physics, 1970, 2(1): 59−86. https://doi.10.1007/bf00628179.

[39] SEMBOSHI S, KANENO Y, TAKASUGI T, HAN S Z, MASAHASHI N. Effect of composition on the strength and electrical conductivity of Cu−Ti binary alloy wires fabricated by aging and intense drawing [J]. Metallurgical And Materials Transactions A−Physical Metallurgy and Materials Science, 2019, 50A: 1389−1396. https://doi.10.1007/s11661-018-5088-z.

[40] MIYAKE J, GHOSH G, FINE M E. Design of high-strength, high-conductivity alloys [J]. Mrs Bulletin, 1996, 21(6): 13−18. https://doi.org/10.1557/S0883769400046005

Cr/Mg 微合金化增强铜钛合金性能的机理

卫 欢[1]，蔚宏利[2]，杜华云[2]，王 骞[2]，周才智[3]，卫英慧[2]，侯利锋[2]

1. 太原理工大学 航空航天学院，太原 030024；
2. 太原理工大学 材料科学与工程学院，太原 030024；
3. College of Engineering and Computing, University of South Carolina, Columbia, SC 29208, USA

摘 要：研究 Cr 和 Mg 元素添加对 Cu−Ti 合金显微组织和性能的影响。采用真空感应熔炼方法制备 Cu−Ti−Cr−Mg 合金。对 Cu−Ti−Cr−Mg 合金在不同时效状态下的显微组织和相组成进行表征，并对材料的硬度和电导率进行测试。结果表明，Cu−Ti−Cr−Mg 合金中的析出顺序类似于二元 Cu−Ti 合金，其中 Cr 和 Ti 在铸造过程中形成金属间化合物 Cr_2Ti。Cr 和 Mg 元素的添加提高合金的硬度。Cu−Ti−Cr−Mg 合金中 Mg 含量的增加导致晶粒细化和连续析出相在早期时效阶段的快速形核，而且 Mg 元素的加入通过沿析出相表面偏析从而阻碍不连续析出相的长大。因此，Cu−4Ti−0.5Cr−1Mg 合金在晶界处表现出有限的不连续析出物，在过时效期间硬度呈现缓慢下降。

关键词：Cu−Ti 合金；微合金化元素；不连续析出相；析出硬化

(Edited by Bing YANG)